JOURNAL OF Materials CHEMISTRY

Dielectric properties and structure of Bi_4NbO_8Cl and Bi_4TaO_8Cl

A. M. Kusainova,[a] S. Yu. Stefanovich,[b] V. A. Dolgikh,[c] A. V. Mosunov,[b] C. H. Hervoches[a] and P. Lightfoot*[a]

[a]*School of Chemistry, University of St Andrews, St Andrews, Fife, UK KY16 9ST. E-mail: pl@st-and.ac.uk*
[b]*Karpov Institute of Physical Chemistry, 103064 Moscow, Russia*
[c]*Department of Chemistry, Moscow State University, 119899 Moscow, Russia*

Received 20th October 2000, Accepted 17th January 2001
First published as an Advance Article on the web 22nd February 2001

The layered intergrowth phases Bi_4MO_8Cl (M = Nb, Ta), structurally related to the well-known Aurivillius phase ferroelectrics, have been studied using SHG and a.c. impedance techniques. Both undergo a polar to centrosymmetric phase ferroelectric-type transition ($T_c = 765$ and 640 K for M = Nb and Ta, respectively). The crystal structure of the low temperature phase of Bi_4NbO_8Cl has been re-analysed, and a tentative structure for Bi_4TaO_8Cl determined, from powder neutron diffraction data. The basic structural features are confirmed, but significant details differ from the previously reported X-ray structure of Bi_4NbO_8Cl.

Introduction

Bismuth-containing oxides exhibit many interesting physical properties, including ferroelectricity in the Aurivillius phases, for example $SrBi_2Ta_2O_9$,[1] and oxide ion conductivity in phases based on $Bi_4V_2O_{11}$ (the so-called BIMEVOX family, also derivatives of the Aurivillius phases)[2] and in δ-Bi_2O_3 itself.[3] In 1986, Ackerman[4] reported the synthesis and structural characterisation of a new family of layered bismuth oxyhalides based on regular intergrowths of two known families of layered materials, the Aurivillius phases, of general formula $[Bi_2O_2][A_{n-1}B_nO_{3n+1}]$,[5] and the Sillén phases of general formula $[Bi_2O_2][X_m]$.[6] Both of these families consist of fluorite-related $[Bi_2O_2]$ layers alternating with either perovskitic or halide layers, in the case of Aurivillius and Sillén phases, respectively. Ackerman's series was nicknamed 'Bipox', for 'bismuth-perovskite-oxyhalide', and consists of a regular layer-stacking of the type $[Bi_2O_2][A_{n-1}B_nO_{3n+1}][Bi_2O_2][X_m]$, represented by its simplest member Bi_4NbO_8Cl (*i.e.* $n = 1$, $m = 1$). Although the single crystal X-ray structure of Bi_4NbO_8Cl (Fig. 1) was determined by Ackerman, no physical properties have been reported. In the light of its structural similarity to the above-mentioned materials, we have studied the electrical properties of this compound, and its Ta analogue, in detail, and here report their interesting ferroelectric behaviour. The structure of Bi_4NbO_8Cl suggested by Ackerman has also been re-analysed using powder neutron diffraction data and, although the essential features are in agreement, significant details are found to differ.

Experimental

Pure polycrystalline samples of Bi_4NbO_8Cl **I** and Bi_4TaO_8Cl **II**, suitable for diffraction studies, were prepared by heating stoichiometric quantities of BiOCl, Bi_2O_3 and Nb_2O_5 in air at 993 K for 24 h. Both materials demonstrate low chemical stability at high temperature which hampers the production of compacted pellets for dielectric measurements. Careful X-ray powder examinations show that both materials may be heated to temperatures higher than 1033 K for only a limited time without partial decomposition. The decomposition product is a Nb-doped variant of δ-Bi_2O_3, of variable composition, exhibiting its strongest peak at $d = 3.17$ Å (corresponding to a cubic unit cell parameter of 5.49 Å). Nevertheless, it appeared that heating for only a short time at this temperature does not seriously damage the samples. Therefore, samples suitable for electrical measurements were prepared initally at 993 K, with subsequent pressing into pellets and sintering at 1073 K for 2 h (for **I**) and 10 h (for **II**). In this way compacted pellets with a density *ca.* 80% of theoretical were obtained in the form of disks of 8 mm diameter and 1 mm thick. A fraction of 5 wt% of the secondary phase (Nb-doped δ-Bi_2O_3) was estimated for **I** after this heat treatment, and less than 10% for **II**, by Rietveld

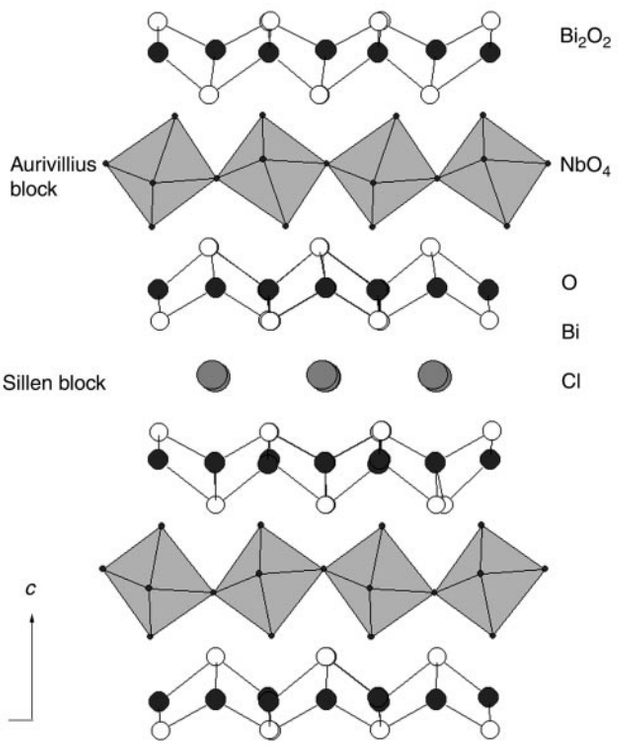

Fig. 1 Crystal structure of the Bipox phase Bi_4NbO_8Cl showing the regular intergrowth of Aurivillius- and Sillén-like units.

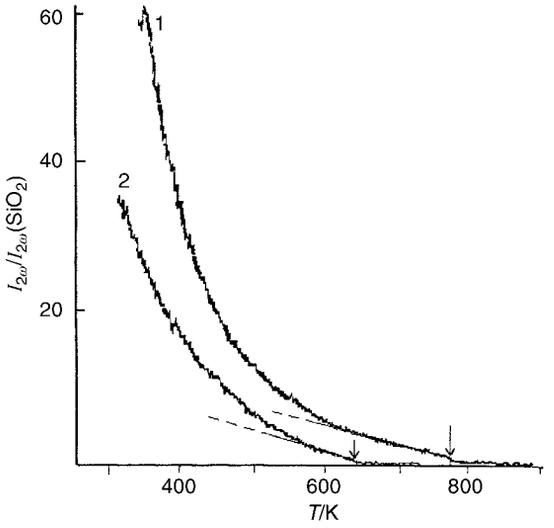

Fig. 2 SHG signal intensities *vs.* temperature for Bi_4NbO_8Cl (1) and Bi_4TaO_8Cl (2) compacted pellets.

analysis of X-ray powder data. Good conducting electrodes with electrical resistance 2–5 Ω were put on both sides of the disks by Pt-paste painting and annealing at 993 K.

Both dielectric constant and electrical conductivity were measured between 300 and 1000 K with PC-controlled a.c. bridges in the frequency range 10^3–10^6 Hz. Second harmonic generation (SHG) tests were carried out in the range 300–900 K in order to establish the temperature range for non-centrosymmetricity for **I** and **II**, and also to trace optical non-linearity behavior in the vicinity of transitions into the centrosymmetric phases. The SHG experiments were carried out using a Nd:YAG solid-state laser operating at wavelength $\lambda_\omega = 1.064$ μm in the Q-switching mode with repetition rate 4 Hz. Both powder and compacted samples (without electrodes) were tested. The laser beam was split into two in order to excite the radiation at doubled frequency ($\lambda_{2\omega} = 0.532$ μm) simultaneously in the sample under investigation that was placed in the electric oven and a reference sample. Thin α-SiO_2 powder with a dispersion of approximately 3 μm was applied as a reference to measure the second harmonic signal intensities. The intensities of the signals from the tested sample ($I_{2\omega}$) and from the reference one [$I_{2\omega}(SiO_2)$] were registered in the backward directions, thus making the signals independent of the thickness of the samples. More background to the SHG technique applied here has been described in detail earlier.[7]

Phase purity was monitored on a Stoe STADI/P powder diffractometer operating in transmission mode and utilising

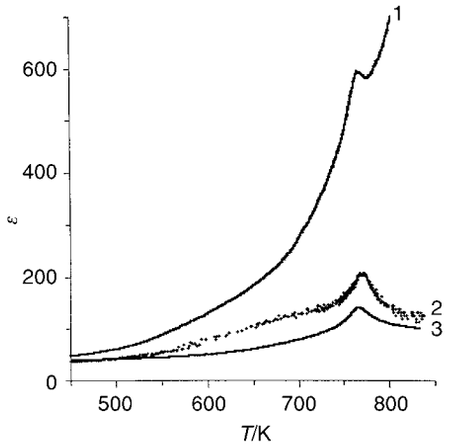

Fig. 3 Dielectric constant temperature dependences for Bi_4NbO_8Cl compacted pellets at frequency 10 (1), 100 (2) and 1000 kHz (3).

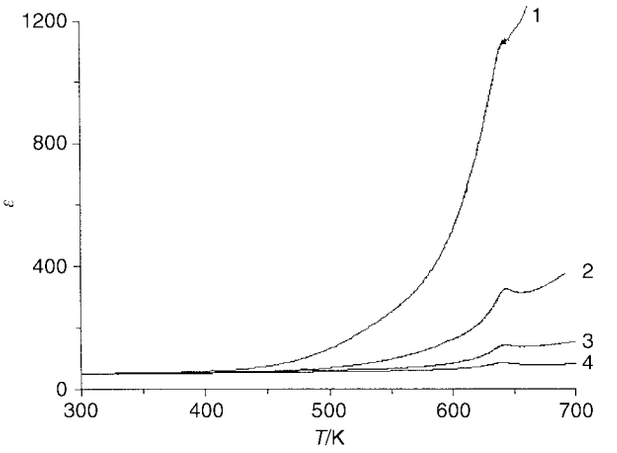

Fig. 4 Dielectric constant temperature dependences for Bi_4TaO_8Cl compacted pellets at frequency 1 (1), 10 (2), 100 (3) and 1000 kHz (4).

monochromated CuKα_1 radiation. Powder neutron diffraction data were collected at 295 K on the high-resolution powder diffractometer HRPD at the ISIS facility, Chilton, UK. Approximately 10 g samples of **I** and **II** were packed into cylindrical vanadium cans and data were collected for 4 h each. The ISIS source operates in energy-dispersive (time-of-flight) mode, with scattered neutrons being detected at fixed detector banks centred at $2\theta = 90$ and 168°. Only the data from the 168° (high-resolution) banks were used for Rietveld refinement, using the GSAS package.[8]

Results and discussion

(i) Non-linear optical and dielectric characterisation

The SHG study of **I** and **II** in both powder and compacted forms demonstrates large second harmonic signals at room temperature (two orders of magnitude higher than for α-quartz), thus unambiguously testifying to strong polar distortion of the Bipox structures. The SHG signals rapidly decrease with temperature showing relaxation of non-centrosymmetricity, though the exact positions of the phase transitions into the centrosymmetric state are difficult to pinpoint from the powder samples. More distinctive results were obtained with the compacted pellets, where a linear decrease of $I_{2\omega}$, expected for proper ferroelectrics, is observed towards the ferroelectric Curie (T_c) temperatures (Fig. 2). Linearity of the SHG response, $I_{2\omega} \approx T_c - T$ is found between 620 and 765 K for compacted samples of **I** and between 570 and 640 K for **II** compacted samples. This behavior may be related to a typical ferroelectric temperature dependence of spontaneous polarization $P_s \approx (T_c - T)^{1/2}$, if we take into account[7] that $I_{2\omega} \approx (\delta^v)^2 \approx P_s^2$. Here δ^v stands for the vector part of the non-linear polarizability which in its turn directly reflects the polar distortion of the crystal structure.[9] Above 765 and 640 K, for **I** and **II** respectively, the SHG signals vanish. So, on the basis of the SHG data alone it is possible to deduce that **I** and **II** undergo ferroelectric-type phase transitions at $T_c = 765$ and 640 K, respectively. Neglecting very small, step-like changes of $I_{2\omega}$ near the Curie temperatures, it may be concluded also that the transitions are second order.

The dielectric constant (ε) for the Bipox compacted pellets **I** and **II** depends strongly on the measuring electric field frequency. At low frequency, 1–10 kHz, dielectric constant anomalies at T_c are hardly seen on the background of a dramatic rise of ε with temperature (Fig. 3 and 4). Nevertheless, the temperature of the dielectric anomalies at any frequency is nearly the same, giving good confirmation of the true origin of the anomalies as crystal structure transformation. At frequencies of 100 and 1000 kHz the $\varepsilon(T)$ maxima at T_c are clearly seen

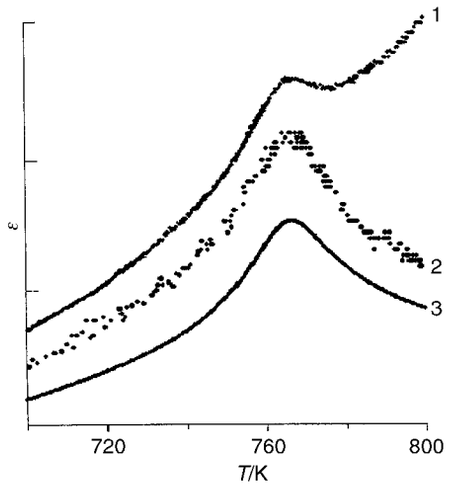

Fig. 5 Dielectric constant maxima near the ferroelectric phase transition in Bi_4NbO_8Cl pellets at frequency 10 (1), 100 (2) and 1000 kHz (3). Note that for ease of comparison the *y*-scale is arbitrary.

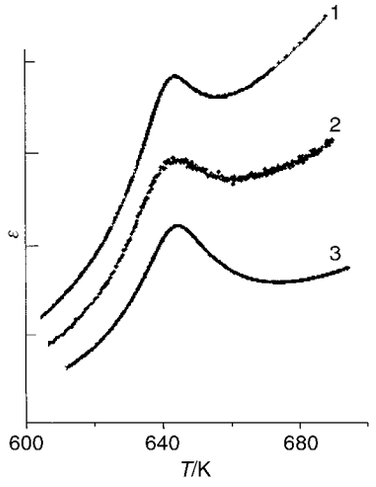

Fig. 6 Dielectric constant maxima near the ferroelectric phase transition in Bi_4TaO_8Cl pellets at frequency 10 (1), 100 (2) and 1000 kHz (3). Note that for ease of comparison the *y*-scale is arbitrary.

to have typically ferroelectric shape (Fig. 5 and 6). Inverse dielectric constant behavior is in accordance with Curie–Weiss law (Fig. 7) and demonstrates only small thermal hysteresis in the heating–cooling cycle, in agreement with the classification of the ferroelectric phase transition as one of nearly second-order. For the pelleted **I** at 100 kHz, above and below the phase

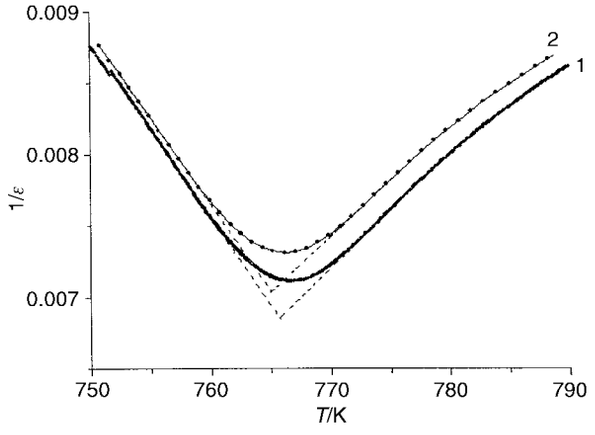

Fig. 7 Inverse dielectric constant at frequency 1000 kHz in Bi_4NbO_8Cl pellets in temperature cycle: heating (1), and cooling (2).

transition, Curie–Weiss constants (C) are 6.1×10^3 and 4.4×10^3 K with their ratio being 1.39, which is less than 2 as required by the phenomenological theory. The C-values for **I** and **II** lay between the values characteristic for order–disorder ($C \approx 10^3$ K) and displacive-type ($C \approx 10^5$ K) ferroelectric structural transformations. Nevertheless, care must be exercised in attributing order–disorder features to the ferroelectric phase transformation in **I** and **II** because the present data have been obtained with pellets of insufficient density. Better processing (for example, hot-pressing of Aurivillius family ferroelectrics[10]) may augment their dielectric and Curie–Weiss constants several times, and make C closer to pure displacive-type quantities.

(ii) Structural characterisation

Ackerman determined the crystal structure of Bi_4NbO_8Cl **I** from single crystal X-ray data in his original report.[4] In parallel with this he reported the structure of an analogue $PbBi_3WO_8Cl$, which, although having the same essential structure, was shown to adopt a higher symmetry tetragonal space group, with no tilting of the octahedral units, whereas **I** itself apparently showed a much more distorted structure with lower symmetry. Since the structures determined in that study were of relatively low precision (errors of 0.07 Å on M–O bond lengths) due to the poor X-ray scattering of oxygen in the presence of heavy metals, we chose to re-analyse the structure of **I** using powder neutron diffraction data, which were expected to give much more definition to the light atom positions in particular. The structure of **II** has also been determined for the first time.

Rietveld refinement commenced using the model of Ackerman for **I**, in space group $P2_1cn$, with $a \approx 5.45$, $b \approx 5.49$, $c \approx 28.8$ Å. This model is a complex superstructure of the 'ideal' structure of $PbBi_3WO_8Cl$ ($a_p \approx 3.87$, $c_p \approx 14.4$ Å) the relationship being $a \approx b \approx \sqrt{2}a_p$, $c \approx 2c_p$, $V \approx 4V_p$. Prior to commencing refinement of this model, therefore, a careful check was made

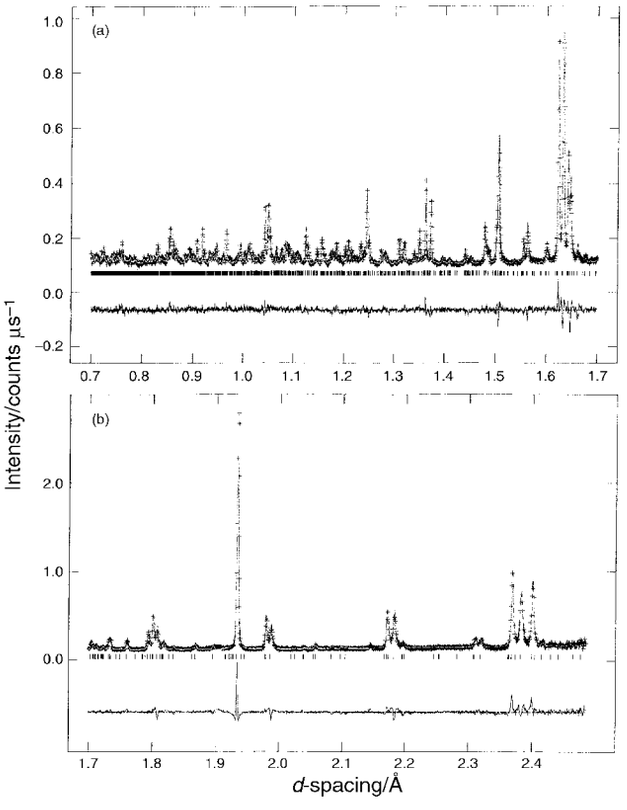

Fig. 8 Final Rietveld fit for the neutron refinement of Bi_4NbO_8Cl in $P2_1cn$.

Table 1 Refined structural parameters for Bi_4NbO_8Cl at 323 K in the true polar space group $P2_1cn$[a] (first line) and centrosymmetric 'parent' space group $Pmcn$[a] (second line), $a=5.4472(1)$, $b=5.4901(1)$, $c=28.8125(6)$ Å

Atom	x[b]	y	z	U_{iso} ($\times 100$)
Nb(1)	0.014(4)	0.243(1)	0.2516(6)	0.6(1)
	0.25	0.241(2)	0.2460(3)	0.5(1)
Bi(1)	0.0[c]	0.814(2)	0.1569(4)	2.2(3)
	0.25	0.785(1)	0.1563(2)	1.0(2)
Bi(2)	0.004(3)	0.253(2)	0.4327(4)	1.5(3)
	0.25	0.250(1)	0.4311(2)	0.3(1)
Bi(3)	0.031(2)	0.779(2)	0.3425(4)	2.7(3)
	0.25	0.817(2)	0.3383(4)	7.2(4)
Bi(4)	0.023(3)	0.254(2)	0.0681(4)	0.6(2)
	0.25	0.253(2)	0.0666(3)	2.7(2)
Cl(1)	0.521(4)	0.238(2)	−0.0011(6)	2.0(1)
	0.75	0.236(2)	0.0027(3)	2.4(1)
O(1)	0.771(4)	0.516(3)	0.3947(5)	0.6(4)
	0.017(2)	0.514(2)	0.3951(3)	0.7(2)
O(2)[d]	0.263(5)	0.495(3)	0.3978(5)	1.2(4)
	—	—	—	—
O(3)	0.767(5)	−0.016(3)	0.3918(5)	1.4(4)
	0.004(3)	−0.011(2)	0.3940(3)	3.6(3)
O(4)[e]	0.267(6)	0.004(3)	0.3940(5)	1.4(4)
	—	—	—	—
O(5)	0.432(3)	0.687(2)	0.3171(4)	0.2(2)
	0.75	0.700(5)	0.318(1)	10.2(8)
O(6)	0.589(5)	0.744(5)	0.1818(10)	8.6(7)
	0.75	0.705(12)	0.182(2)	21.7(20)
O(7)	0.299(4)	0.024(3)	0.2358(5)	2.4(4)
	0.502(4)	−0.011(4)	0.2400(5)	10.1(4)
O(8)[f]	−0.200(5)	−0.055(3)	0.2590(7)	4.3(4)
	—	—	—	—

[a]For $P2_1cn$: $\chi^2=3.65$, $R_{wp}=0.065$; for $Pmcn$: $\chi^2=5.55$, $R_{wp}=0.080$. [b]There is a shift of $\Delta x=0.25$ between the two settings. [c]Fixed to define origin of polar axis. [d]Equivalent to O(1) in $Pmcn$. [e]Equivalent to O(3) in $Pmcn$. [f]Equivalent to O(7) in $Pmcn$.

Table 2 Refined structural parameters for Bi_4TaO_8Cl at 298 K, space group $P2_1cn$, $a=5.4589(2)$, $b=5.5044(2)$, $c=28.6998(9)$ Å

Atom	x	y	z	U_{iso} ($\times 100$)
Ta(1)	−0.003(4)	0.248(2)	0.2483(5)	−0.6(1)
Bi(1)	0.0[a]	0.832(2)	0.1570(4)	1.2(2)
Bi(2)	0.006(4)	0.251(2)	0.4313(4)	0.1(2)
Bi(3)	0.025(3)	0.743(2)	0.3425(4)	1.6(2)
Bi(4)	0.016(4)	0.249(2)	0.0670(4)	0.9(2)
Cl(1)	0.509(5)	0.254(2)	−0.0002(5)	1.7(1)
O(1)	0.772(6)	0.516(4)	0.394(1)	0.9(9)
O(2)	0.264(6)	0.496(3)	0.395(1)	0.3(7)
O(3)	0.768(6)	0.003(4)	0.395(1)	1.2(8)
O(4)	0.269(6)	0.006(3)	0.395(1)	−0.3(7)
O(5)	0.420(5)	0.712(3)	0.3196(7)	2.0(6)
O(6)	0.589(5)	0.701(3)	0.1856(7)	1.9(6)
O(7)	0.301(6)	0.061(1)	0.240(1)	3.9(8)
O(8)	−0.221(7)	−0.048(4)	0.2624(9)	3.6(7)

[a]Fixed to define origin of polar axis.

both for the doubled c-axis, and the distortion in the ab plane (a C-centred supercell may be expected for this distortion). Both the doubling of the c-axis and the lowering of supercell symmetry from C-centred to primitive were confirmed from the neutron data by the presence of the peaks (131) at 1.74 Å and (135) at 1.66 Å, and by the peak (124) at 2.32 Å. Rietveld refinement consisted of a total of 68 variable parameters refined against 1807 reflections and 4402 data points in the d-spacing range $0.66<d<2.5$ Å. The parameters refined were scale factor, a six-parameter background function, two peak-shape coefficients (a pseudo-Voigt/double-exponential convolution was used), detector zero-point, three lattice parameters and coordinates and isotropic temperature factors for the 14 atoms in the asymmetric unit [the x-coordinate of Bi(1) was fixed in order to define the origin of the polar axis]. Convergence of this model was achieved leading to final agreement factors, $R_{wp}=0.065$, $\chi^2=3.65$ (Fig. 8) for **I** and $R_{wp}=0.179$, $\chi^2=27.5$ for **II**. Final refined atomic coordinates are given in Tables 1 and 2, and selected bond distances and angles in Table 3. We note that the relatively high agreement factors for **II** are due to a slight systematic broadening of the ($0kl$) reflections, compatible with a very subtle lowering of symmetry to monoclinic (space group $P2_111$, a-unique). This reduction in symmetry leads to a very complex structure, with 83 refinable atomic coordinates. We were unable to obtain a satisfactory refinement of the structure using this model, and suggest that the data in Tables 2 and 3 represent a satisfactory model of the structure, with this *caveat* in mind.

The distortion of these structures from the 'ideal' symmetry, discussed above, is subtle but genuine. For example, for **I**, refinements in the $5.45\times5.49\times14.4$ Å subcell, in space group

Table 3 Selected bond distances (Å) and angles (°) for Bi_4MO_8Cl (**I**: M = Nb; **II**: M = Ta)

	I	**II**
M(1)–O(5)	2.05(2)	2.00(3)
M(1)–O(6)	1.96(3)	1.98(3)
M(1)–O(7)	2.01(2)	1.97(3)
	1.97(2)	2.05(3)
M(1)–O(8)	2.02(2)	2.06(3)
	1.94(2)	1.93(3)
Bi(1)–O(1)	2.37(2)	2.31(3)
Bi(1)–O(2)	2.27(2)	2.17(3)
Bi(1)–O(3)	2.71(2)	2.76(3)
Bi(1)–O(4)	2.58(2)	2.65(2)
Bi(1)–O(5)	2.21(1)	2.24(2)
Bi(1)–O(6)	2.38(3)	2.50(2)
Bi(1)–O(7)	3.02(2)	3.16(3)
Bi(1)–O(8)	3.22(3)	3.33(3)
Bi(2)–Cl(1)	3.25(2)	3.35(2)
	3.40(2)	3.38(2)
	3.45(2)	3.37(1)
	3.32(2)	3.40(1)
Bi(2)–O(1)	2.21(2)	2.22(3)
Bi(2)–O(2)	2.18(2)	2.21(2)
Bi(2)–O(3)	2.29(2)	2.16(3)
Bi(2)–O(4)	2.27(2)	2.23(2)
Bi(3)–O(1)	2.52(2)	2.37(3)
Bi(3)–O(2)	2.56(2)	2.41(3)
Bi(3)–O(3)	2.31(2)	2.50(3)
Bi(3)–O(4)	2.32(2)	2.47(3)
Bi(3)–O(5)	2.36(2)	2.26(2)
Bi(3)–O(6)	3.04(3)	3.11(2)
	2.67(3)	2.67(2)
Bi(3)–O(7)	2.94(2)	2.85(4)
Bi(3)–O(8)	2.86(3)	2.90(3)
Bi(4)–Cl(1)	3.38(2)	3.37(2)
	3.37(2)	3.31(2)
	3.32(2)	3.37(2)
	3.39(1)	3.34(2)
Bi(4)–O(1)	2.17(2)	2.21(3)
Bi(4)–O(2)	2.24(2)	2.24(3)
Bi(4)–O(3)	2.17(2)	2.25(3)
Bi(4)–O(4)	2.24(2)	2.24(3)
O(5)–M(1)–O(6)	172(1)	167(1)
O(5)–M(1)–O(7)	82(1)	90(1)
	100(1)	98(1)
O(5)–M(1)–O(8)	82(1)	90(1)
	96(1)	94(1)
O(6)–M(1)–O(7)	94(1)	81(1)
	87(1)	95(1)
O(6)–M(1)–O(8)	89(1)	82(1)
	91(1)	92(1)
O(7)–M(1)–O(7)	165(1)	154(2)
O(7)–M(1)–O(8)	89(1)	96(1)
	72(1)	67(1)
	106(1)	109(1)
	93(1)	87(2)
O(8)–M(1)–O(8)	161(1)	163(2)
M(1)–O(7)–M(1)	152(3)	149(6)
M(1)–O(8)–M(1)	156(4)	153(4)

Table 4 Bond valence sum analysis for **I** and **II**

Atom	**I** (present work)	**I** (Ackerman)	**II** (present work)
M(1)	4.84	5.26	4.89
Bi(1)	2.91	3.20	2.88
Bi(2)	3.16	2.90	3.34
Bi(3)	2.73	5.23	2.77
Bi(4)	3.39	3.39	3.15
Cl(1)	0.75	0.85	0.74
O(1)	2.34	2.54	2.48
O(2)	2.38	2.79	2.65
O(3)	2.15	2.85	2.00
O(4)	2.10	2.51	1.95
O(5)	1.94	2.15	2.19
O(6)	1.69	3.27	1.46
O(7)	1.76	1.82	1.77
O(8)	1.83	1.20	1.81

$P2_1mn$ give a best fit around $\chi^2 \approx 6$; moreover, the imposition of mirror symmetry on several atoms leads to unacceptably high thermal parameters. Similarly, refinement in the 'parent' centrosymmetric version of the $5.45 \times 5.49 \times 28.8$ Å cell, in space group *Pmcn* leads to anomalously large thermal parameters, in particular for the oxygen atoms of the NbO_6 octahedron; these are given for comparison with the true structure in Table 1. From this comparison it may be inferred that the displacements of these oxygen atoms offer the most significant contribution to the overall polarisation. A comparison with the structural model of Ackerman can also be made at this point. That model, although obtained from single crystal X-ray diffraction data, showed not only very high errors on the derived geometry, but also some anomalously short bond lengths, for example, Bi(3)–O(3) = 1.90 Å. The relative quality of the two refinements can be judged by bond valence sum analysis,[11,12] which is presented in Table 4. This analysis clearly shows some very unusual bond valence sums for the Ackerman model, in particular the values of 5.23 and 1.20 for Bi(3) and O(8), respectively, and underlines the significantly improved precision for light atom parameters obtained with neutron rather than X-ray scattering. It is interesting to note, however, that in the present models two unusual points can be observed in these data. Firstly, the oxygens within the $[Bi_2O_2]$ layers, specifically O(1) and O(2), are significantly *over*-bonded, for both **I** and **II** and, secondly, the apical oxygen O(6) is grossly *under*-bonded in both cases. In the latter case this value is critically dependent on the length of the apical Nb(1)–O(6) bond, which was reported as 1.72(7) Å by Ackerman, but 1.96(3) Å for **I** in the present study. In fact, from the present study the $M(1)O_6$ octahedra are quite regular, which may be contrasted with the behaviour in related Aurivillius phases such as Bi_2WO_6[13] and $Bi_2ANb_2O_9$ (A = Ca, Sr, Ba)[14] which in all cases display a significant off-centre shift of the octahedral M atom, and M–O bond lengths in the more extensive range of *ca.* 1.8–2.2 Å. The precise reasons for these differences are not yet clear, but it is apparent that the octahedral M(1) atoms in the present structures are able to accommodate their bonding requirements without a need for such an off-centre displacement. In detail, the structures of **I** and **II** are very similar, with little difference in either octahedral tilting or distortion.

Conclusions

We have shown that the two simplest members of the Aurivillius–Sillén intergrowth family ('Bipox' phases), Bi_4MO_8Cl (M = Nb, Ta), exhibit ferroelectric properties similar to many oxides in the Aurivillius family.

The crystal structures of both Bi_4NbO_8Cl and Bi_4TaO_8Cl have been determined from powder neutron diffraction data. The structure obtained for Bi_4NbO_8Cl improves considerably on the precision obtained in the previously reported single crystal X-ray study, though the broad structural features are in agreement. Both structures display the same mode of complex distortion, leading to a considerable lowering of symmetry from the 'ideal' structure type. It may be anticipated that the structures will tend towards more ideal symmetry near the phase transition temperature, and above this temperature will adopt one of the simpler possible subcells. A variable temperature powder neutron diffraction experiment is planned in order to study the phase transition in more detail.

Acknowledgements

We would like to thank INTAS for supporting this work under grant 96-1324, and the EPSRC for a Project Studentship (to C. H. H) and for provision of neutron diffraction facilities at ISIS. We thank Dr K. S. Knight and Dr R. M. Ibberson for help in the neutron data collection.

References

1 C. A. P. de Araujo, J. D. Cuchlaro, L. D. McMillan, M. Scott and J. F. Scott, *Nature (London)*, 1995, **374**, 627.
2 F. Abraham, M. F. Debruille-Gresse, G. Mairesse and G. Nowogrocki, *Solid State Ionics*, 1988, **28–30**, 529.
3 H. L. Tuller and A. S. Nowick, *J. Electrochem. Soc.*, 1975, **122**, 255.
4 J. F. Ackerman, *J. Solid State Chem.*, 1986, **62**, 92.
5 B. Frit and J. P. Mercurio, *J. Alloys Compd.*, 1992, **188**, 27.
6 V. A. Dolgikh and L. N. Kholodkovskaya, *Russ. J. Inorg. Chem.*, 1992, **37**, 488.
7 S. Yu. Stefanovich, in *Proceedings of the European Conference on Lasers and Electro-Optics*, (Abstracts), IEEE, Amsterdam, 1994, pp. 249–250.
8 A. C. Larson and R. B. von Dreele, Los Alamos National Laboratory Report No. LA-UR-86-748, 1987.
9 S. K. Kurtz and T. T. Perry, *J. Appl. Phys.*, 1968, **39**, 3798.
10 K. R. Kendal, C. Navas, J. K. Thomas and H.-C. zur Loye, *Chem. Mater.*, 1996, **8**, 642.
11 I. D. Brown and D. Altermatt, *Acta Crystallogr., Sect. B*, 1985, **41**, 244.
12 N. Brese and M. O'Keeffe, *Acta Crystallogr., Sect. B*, 1991, **47**, 192.
13 K. S. Knight, *Mineral. Mag.*, 1992, **56**, 399.
14 S. M. Blake, M. J. Falconer, M. McCreedy and P. Lightfoot, *J. Mater. Chem.*, 1997, **7**, 1609.